Differentiation of mafic magma in a continental crust-to mantle transition zone

JOURNAL OF PETROLOGY | VOLUME 42 | NUMBER 1 | PAGES 189–206 | 2001

Differentiation of Mafic Magma in a Continental Crust-to-Mantle Transition Zone

JÖRG HERMANN[1]*, OTHMAR MÜNTENER[1]† AND DETLEF GÜNTHER[2]‡

[1]INSTITUT FÜR MINERALOGIE UND PETROGRAPHIE, ETH ZÜRICH, CH 8092 ZÜRICH, SWITZERLAND
[2]INSTITUT FÜR ISOTOPENGEOLOGIE UND MINERALISCHE ROHSTOFFE, ETH ZÜRICH, CH 8092 ZÜRICH, SWITZERLAND

RECEIVED NOVEMBER 17, 1999; REVISED TYPESCRIPT ACCEPTED JUNE 27, 2000

The Braccia gabbro complex (Eastern Central Alps, Northern Italy) intruded the boundary between the Adriatic lowermost continental crust and the subcontinental upper mantle in Permian times. The gabbro complex consists mainly of gabbro–norites with minor dykes of quartz diorite and Fe–Ti–P-rich diorite. The gabbro–norites contain abundant cumulus clino- and orthopyroxene and only small amounts of olivine, indicating crystallization at high pressure ($\sim 1{\cdot}0$ *GPa). Slow, near-isobaric cooling of the gabbro erased compositional zoning of major and trace elements in magmatic minerals. Bulk-rock composition and the combination of* mg*-number in pyroxenes and modelling of mineral trace element data permit us to track the trace element enrichment in minerals and whole rocks. Some trace element rich gabbros represent frozen liquids, whereas others are cumulates formed from highly differentiated residual liquids. Differentiation of the gabbro complex is mainly driven by fractional crystallization of pyroxenes and plagioclase, resulting in a tholeiitic differentiation trend. The trace element composition of the parental melt was calculated from the most primitive pure cumulate found in the Braccia gabbro complex. This parental melt is similar to transitional mid-ocean ridge basalts, although the Braccia gabbro crystallized at the base of the continental crust. It is suggested that the parental melt originated from decompression melting of upwelling mantle within the spinel peridotite field. Thus, a thinned lithosphere with a high geothermal gradient existed at the northern part of the African plate in Permian times.*

KEY WORDS: *differentiation; gabbro; geochemistry; lower crust; mafic underplating*

*Corresponding author. Present address: Research School of Earth Sciences, ANU, Canberra, A.C.T. 0200, Australia. Telephone: +61-2-6249-3416. Fax: +61-2-6249-5989.
E-mail: Joerg.Hermann@anu.edu.au
†Present address: Geologisches Institut, ETH Zürich, CH 8092 Zürich, Switzerland.
‡Present address: Institut für Anorganische Chemie, ETH Zürich, CH 8092 Zürich, Switzerland.

INTRODUCTION

Much of the understanding of phase relations and differentiation processes in tholeiitic mafic rocks comes from detailed investigations of the oceanic crust (e.g. Langmuir *et al.*, 1992) and from experiments related to melting and crystallization of such rock types (Green & Ringwood, 1967; Elthon & Scarfe, 1984). In continental crust, tholeiitic magma crystallization is well known in layered mafic complexes that intruded at upper-crustal levels (i.e. Skaergaard intrusion, MacBirney, 1975). Much less is known about the magmatic evolution of gabbros, which were emplaced at the continental crust–mantle transition. Differentiation processes can be obscured by extensive contamination of the mafic magma with partial crustal melts (e.g. Ivrea Zone, Voshage *et al.*, 1990; Mazzuchelli *et al.*, 1992*a*; Sinigoi *et al.*, 1994). Another problem is that the trapped interstitial liquid, which is recognizable in upper-crustal gabbros (Tribuzio *et al.*, 1999*b*), tends to equilibrate with the earlier formed cumulus phases (Mazzuchelli *et al.*, 1992*b*). Cawthorn (1996) demonstrated that such re-equilibration leads to enrichment especially of incompatible elements in the cumulus phases and this enrichment may be wrongly interpreted as an effect of differentiation.

In this paper we present field, petrologic and chemical data for the Braccia gabbro complex (Val Malenco, Eastern Central Alps, Fig. 1) in order to constrain differentiation of mafic magma at the crust–mantle boundary. The Braccia gabbro displays primary intrusive contacts with the adjacent peridotites and pelitic granulites (Müntener & Hermann, 1996; Hermann *et al.*, 1997). Pressure

estimates in the country rocks indicate ~1·0 GPa during intrusion (Hermann *et al.*, 1997; Müntener *et al.*, 2000). Age determinations of the gabbro and of the partial melt segregates in the pelitic granulites yield Permian ages that are the same within error (Hansmann *et al.*, 1996; Hermann *et al.*, 1997). Through detailed mapping of pre-Alpine and Alpine structures it is possible to infer the geometry of the Braccia gabbro intrusion in Permian times. On the basis of these data we conclude that the Braccia gabbro intruded at the crust–mantle boundary at ~35 km depth and that the underlying peridotite represents the lithospheric mantle at the time of intrusion (Müntener & Hermann, 1996; Hermann *et al.*, 1997). During subsequent Jurassic rifting, the rocks of the crust-to-mantle transition were exhumed to the Tethyan ocean floor (Trommsdorff *et al.*, 1993; Hermann & Müntener, 1996). The exhumed mantle rocks were partly cross-cut and overlain by the mid-ocean-ridge-type basalts of the Forno unit (Fig. 1; Puschnig, 1998). During Cretaceous convergence the rocks were integrated into the Alpine nappe stack and most of the gabbros recrystallized under Alpine epidote–amphibolite facies conditions. However, the preserved magmatic minerals in the area of Mt. Braccia offer the possibility of investigating the magmatic evolution of a mafic intrusion at the base of the continental crust.

In this study petrography, whole-rock data, trace element mineral chemistry obtained by laser ablation–ICP-mass spectrometry (LAM-ICP-MS) and rare earth element (REE) modelling are used to unravel the combined effects of differentiation and trapped liquid in slowly cooling, deep-seated mafic rocks. Our results show that *in situ* differentiation (Langmuir, 1989) can account for the chemical variability of mafic rocks in the Braccia gabbro. We discuss the implications of the calculated parental melt for the thermal and tectonic regime at the time of the gabbro intrusion.

ROCK TYPES AND FIELD RELATIONS

The Braccia gabbro consists mainly of clinopyroxene, orthopyroxene and plagioclase and is thus classified as gabbro–norite. The rocks locally display magmatic layering as a result of modal variations of pyroxene and plagioclase, and have abundant pyroxenite cumulates. Only a few gabbros contain significant proportions of olivine, but ultramafic olivine–Cr-spinel cumulates were not found. Most of the gabbros have been affected by subsolidus, high-temperature deformation. However, undeformed lenses with magmatic features have been found (Hermann & Müntener, 1996). Subsolidus cooling did not change the mineral paragenesis in the gabbros (Müntener *et al.*, 2000). Spinel and garnet coronas are restricted to a few olivine-bearing samples. Coronas form a small rim of ~100 μm around centimetre-sized igneous minerals. Coronitic spinel is Cr free and always associated with coronitic pyroxenes that are texturally and chemically different from the igneous minerals (Müntener *et al.*, 2000). Minerals in the studied rocks are compositionally unzoned. These observations indicate that the primary magmatic mineral assemblage is largely preserved; however, it has to be tested to what extent the mineral composition can be used to constrain igneous processes.

Two gabbro and three diorite types have been mapped (Fig. 1). The (olivine) gabbro–norite (Mg gabbro) is the most widespread gabbro type and locally displays a modal layering (Müntener & Hermann, 1996). Large euhedral pyroxenes in undeformed lenses indicate an early crystallization (Fig. 2a). Euhedral olivine is rare and forms flaser type aggregates. Ti-pargasite and rare ilmenite occur interstitially. From textural relationships it is not always evident if Ti-pargasite formed during retrograde metamorphic hydration or if it represents a late crystallizing phase. The ilmenite gabbro–norite (Fe gabbro) is often fine grained and darker than the Mg gabbro. There is a continuous transition from Mg to Fe gabbros. However, in some places Fe gabbro dykes cross-cut the Mg gabbro, and Mg gabbro xenoliths occur within the Fe gabbro. The Fe gabbro contains significant amounts of ilmenite and occasionally accessory apatite. Olivine occurs only as rare, small crystals whereas pyroxenes form large idiomorphic grains (Fig. 2b). Ilmenite, Ti-pargasite and occasionally green spinel fill the interstices, suggesting that they represent late-crystallized magmatic phases (Fig. 2b). Highly differentiated diorites occur generally as dykes or small bodies within the Fe gabbro. The pyroxene–ilmenite–amphibole diorite (Fe–Ti diorite) is fine grained and nearly black. Some dykes, occurring mainly in the overlying lower crust, are characterized by euhedral Ti-pargasite and abundant ilmenite and apatite. Occasionally, several tens of zircons per thin section were found. Fine-grained (quartz) diorite (qtz diorite) contains variable proportions of quartz flasers. Orthopyroxene and ilmenite are the only mafic minerals in this rock type.

WHOLE-ROCK COMPOSITION

The compositions of various gabbro and diorite types are given in Table 1. The evolution from Mg to Fe gabbros to diorite dykes is well reflected in the change of bulk-rock *mg*-number (Fig. 3). The SiO_2 content remains constant from Mg to Fe gabbro, which is characteristic of tholeiitic differentiation. The incompatible elements such as Ti, P, Ba and Zr became enriched with decreasing whole-rock *mg*-number (Fig. 3). The concentrations of compatible elements Cr and Ni do not exceed a few

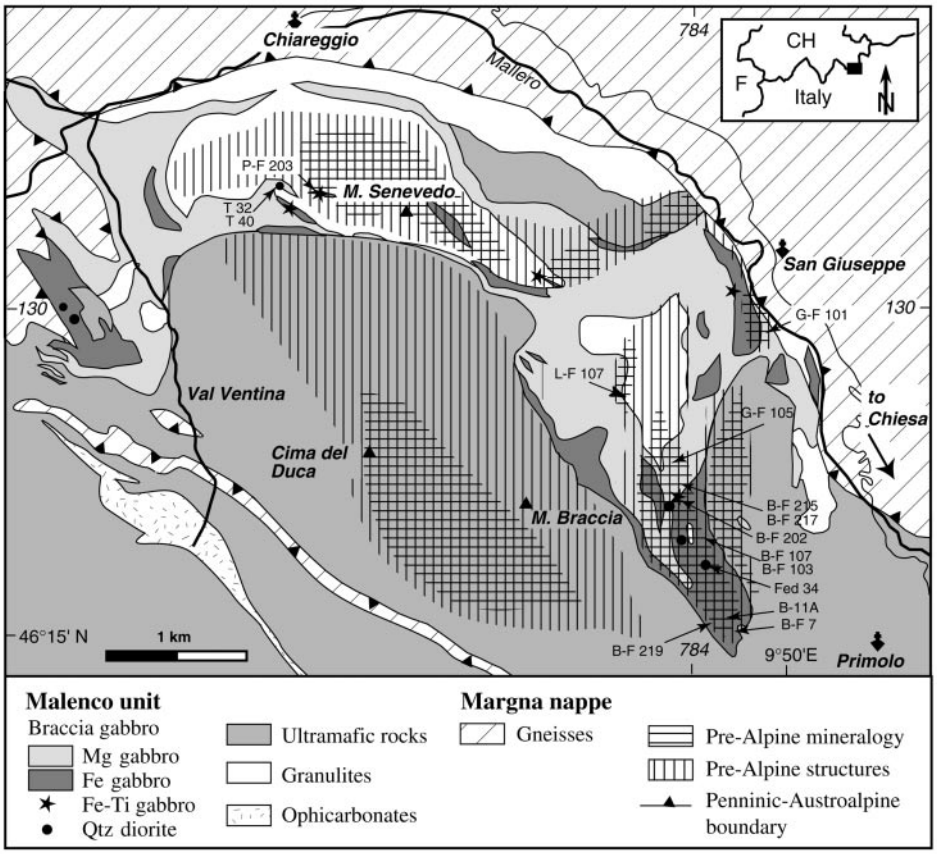

Fig. 1. Geological map of the Braccia gabbro showing the distribution of different gabbro types. Areas with preserved pre-Alpine structures and mineralogy are indicated. The locations of samples are indicated by arrows. Numbers (784 and 130) refer to Swiss grid coordinates. Inset shows location of the area at the border between Switzerland and Italy.

hundred ppm even in the gabbros with the highest *mg*-number (Table 1).

The highly differentiated Fe–Ti diorites and Qtz diorites have a similar low *mg*-number but display a complementary evolution in SiO_2 and trace element concentration (Fig. 3). The high field strength elements (HFSE) such as Ti, Y, Zr and P have a higher concentration within the SiO_2-poor Fe–Ti gabbros and are incorporated in Ti-pargasite and accessory phases (ilmenite, apatite and zircon). The large ion lithophile elements (LILE) such as Ba and K are much more abundant in the SiO_2-rich Qtz diorites and are mostly incorporated in plagioclase.

Rare earth element (REE) concentrations strongly increase from Mg to Fe gabbros (Fig. 4a). Plagioclase-rich gabbros are enriched in light REE (LREE) with respect to heavy REE (HREE) (L-F 107) whereas pyroxene-rich gabbros show the opposite pattern (B-F 215). Most of the gabbros display a positive Eu anomaly that decreases with decreasing *mg*-number of the gabbros. The Fe gabbro (B-F 107) displays no Eu anomaly despite similar proportions of plagioclase to the Mg gabbro (G-F 105). This indicates that sample B-F 107 most probably does not represent a pure cumulate. The Fe–Ti diorites have a very similar pattern to the Fe gabbros but REE contents are slightly higher. The amount of REE in the (qtz) diorites strongly decreases with decreasing proportions of mafic minerals (Table 1). The REE pattern in sample Fed 34 is controlled by the high proportions of plagioclase. This evolution is similar to that of the HFSE, which are also much less abundant in qtz diorite than in Fe–Ti gabbro (Fig. 3).

MINERAL CHEMISTRY

Pyroxenes

The *mg*-number of pyroxenes decreases from Mg to Fe gabbro to highly differentiated dykes (Table 2, Fig. 5a). The Mn content of the pyroxenes increases with that of the whole rock (Fig. 5a). Except for sample B-F 103, clinopyroxene displays a high Na_2O content independent of the *mg*-number (Table 3). The Fe–Mg partitioning between clino- and orthopyroxene changes slightly from

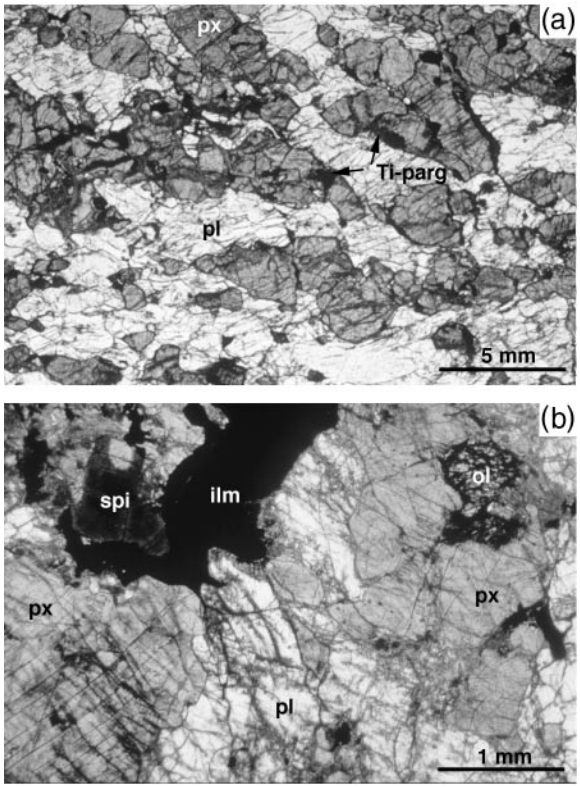

Fig. 2. (a) Mg gabbro G-F 105 consists mainly of pyroxenes (px) and plagioclase (pl). Ti-pargasite (Ti-parg) occurs interstitially. (b) Fe gabbro B-F 7: large pyroxenes (px) and plagioclase are the major constituents of the Fe gabbro–norites. Olivine is rare and forms small grains. Ilmenite (ilm) and spinel (spi) fill interstices.

Mg to Fe gabbros (Fig. 5b). In Mg gabbros the K_d of cpx–opx ($Fe/Mg_{cpx} - Fe/Mg_{opx}$) is $\sim 0{\cdot}8$ whereas in Fe gabbro the K_d is 0·6.

The amount of Y, Zr and REE in both ortho- and clinopyroxene (Table 3) strongly increases with decreasing *mg*-number (Fig. 6a and b). Pyroxenes from sample G-F 105 have low REE contents characterizing this sample as a primitive gabbro type. There is no Eu anomaly observable in pyroxenes from Mg gabbros. In contrast, pyroxenes from Fe gabbros display a negative Eu anomaly. The partitioning of REE between ortho- and clinopyroxene decreases with increasing atomic number (Fig. 7a). There is no systematic change in the partitioning with decreasing *mg*-number of the pyroxenes.

Plagioclase

Plagioclase is usually equigranular and unzoned with a K-feldspar component <2%. The anorthite content of plagioclase does not exceed An_{60} and is generally between An_{50} and An_{55} in the Mg gabbro. In the Fe gabbro, plagioclase varies between An_{40} and An_{50}. Plagioclase in highly differentiated Fe–Ti diorites and in the Qtz diorite displays a lower anorthite content of $An_{33–40}$.

The REE pattern of plagioclase is characterized by enrichment of LREE relative to middle REE (MREE) and HREE, and by a positive Eu anomaly (Fig. 6c). In all gabbro–norites the HREE were below detection limit. Whereas the evolution from Mg to Fe gabbros is only poorly reflected by changing An content, REE, Ba and Pb increase by a factor of 2–8 from sample G-F 105 to sample B-F 7 (Table 3).

Ti-pargasite

The *mg*-number of pargasite is positively correlated with that of pyroxenes (Fig. 5b) and changes from Mg to Fe gabbro to Fe–Ti diorites. In contrast to the pyroxenes, other major elements do not change systematically with *mg*-number.

Similar to the main minerals pyroxene and plagioclase, the REE in Ti-pargasite increase during differentiation (Fig. 6, Table 3). In sample P-F 203, Ti-pargasite is the dominant mafic phase and displays a significant negative Eu anomaly. Ba and Rb are preferentially incorporated in Ti-pargasite with respect to plagioclase, whereas Sr displays the opposite feature. From the textural relationships of Ti-pargasite in the Mg gabbros it is not clear if it formed during a late magmatic stage or represents an early metamorphic overgrowth on magmatic pyroxene. The significantly higher amount of trace elements and the systematically lower *mg*-number with respect to clinopyroxene strongly argues for late magmatic crystallization (e.g. Tribuzio *et al.*, 1999*b*).

Ilmenite

The Mg and Mn content of ilmenite varies considerably but does not show a systematic change from Mg to Fe gabbros. In contrast, Nb and Ta in ilmenite strongly increase from the Mg gabbro to the highly differentiated Fe–Ti diorite (Table 3). Abundant trace elements are V, Cr, Ni and Zn, whereas the REE are at or below detection limit.

Olivine

Olivine is less abundant in the gabbros and much more altered during the subsequent metamorphic evolution than the pyroxenes. The *mg*-number and NiO content of olivine vary from the Mg gabbro flasers (0·8–0·77 and 0·11–0·08 wt %, respectively) to the small olivine grains in the Fe gabbro (0·73 and <0·05 wt %, respectively).

Table 1: Representative composition and mineral content of different gabbro and diorite types

	Mg gabbro				Fe gabbro			Fe–Ti diorite		Qtz diorite		
Sample:	G-F 105	L-F 107	B-F 217	B-F 215	B-F 7	B-F 11A	B-F 107	P F 203	B-F 202	T40*	T32*	Fed 34
Major elements determined by XRF (wt %)												
SiO_2	50·86	49·31	52·92	50·48	50·12	47·72	48·60	46·48	42·80	52·21	57·80	61·00
TiO_2	0·87	0·14	0·46	0·84	1·02	2·49	2·21	3·39	4·04	0·80	0·51	0·28
Al_2O_3	16·06	23·38	16·17	15·82	17·68	15·98	14·69	16·98	11·71	18·15	17·84	19·50
Fe_2O_3†	7·00	4·78	7·99	6·57	9·42	12·76	12·26	12·97	20·23	8·94	6·38	4·14
MnO	0·14	0·06	0·16	0·13	0·14	0·19	0·20	0·19	0·35	0·10	0·09	0·10
MgO	9·78	7·61	10·19	8·90	7·99	7·56	7·11	5·13	7·19	5·49	3·77	2·43
CaO	11·48	10·17	9·01	13·02	9·98	9·84	9·18	9·77	9·58	8·64	6·05	6·16
Na_2O	2·30	3·09	2·53	2·42	3·24	2·32	2·02	3·47	1·42	2·89	3·98	4·75
K_2O	0·12	0·10	0·18	0·11	0·21	0·37	0·28	0·78	0·14	0·56	0·28	0·41
P_2O_5	0·02	0·02	0·02	0·02	0·03	0·20	0·32	0·45	0·87	0·10	0·13	0·02
LOI	0·06	0·92	0·18	0·80	0·19	0·00	0·00	0·34	0·93	1·30	1·76	0·62
Total	98·8	99·6	99·9	99·2	100·1	99·5	96·9	100·0	99·3	99·2	98·6	99·4
mg-no.	0·73	0·76	0·72	0·73	0·63	0·54	0·53	0·44	0·41	0·55	0·54	0·54
Mode												
qtz										3	12	13
pl	55	75	54	55	52	54	53	42	(40)	(64)	(66)	74
cpx	21		10	27	13	13	14	(15)	(14)	(6)		
opx	21	12	33	14	25	19	27		(29)	(23)	(18)	12
ol		12			5	6						
Ti-parg	2	1	2	2	tr	tr	1	35	5			
spi					3							
ilm	tr		1	2	2	5	4	5	8	2	1	1
bt		1										
ap		tr	1	2	4	tr	tr					
% alter.	5	30	15	35	5	3	3	25	90	95	95	25
Trace elements determined by XRF (ppm)												
F	237	297	117	208	123	164	<50	902	346	305	260	<50
Ba	32	23	47	39	81	120	159	210	<10	215	153	302
Rb	<3	<3	<3	<3	<3	<3	<3	5	4	<3	<3	<3
Sr	233	377	273	240	265	280	212	530	47	376	645	455
Pb	<5	<5	<5	<5	<5	<5	<5	<5	<5	<5	<5	<5
Nb	<5	<5	<5	<5	<5	<5	<5	20	34	<5	<5	<5
Y	<3	<3	<3	7	5	23	32	26	41	13	<3	<3
Zr	<4	<4	9	22	25	56	122	226	603	43	11	<4
V	307	<16	152	256	217	325	286	397	246	210	132	64
Cr	477	<18	360	399	286	144	300	36	199	83	41	<18
Ni	101	128	68	96	82	81	48	31	92	33	14	14
Co	24	14	21	23	42	54	44	77	134	19	<11	13
Cu	<8	<8	<8	12	20	27	25	<8	260	<8	<8	<8
Zn	30	26	48	33	63	85	99	130	144	92	75	33
Ga	8	8	10	9	12	16	<4	22	14	16	12	15
Sc	45	<2	31	50	29	36	41	33	74	34	16	7
S	<50	<50	<50	241	512	1318	1461	<50	<50	<50	<50	<50

Table 1: continued

	Mg gabbro				Fe gabbro			Fe–Ti diorite		Qtz diorite		
Sample:	G-F 105	L-F 107	B-F 217	B-F 215	B-F 7	B-F 11A	B-F 107	P F 203	B-F 202	T40*	T32*	Fed 34
Trace elements determined by ICP-MS (ppm)												
La	0·63	0·95	1·1	1·4	3·1	5·1	14	30	16	14	17	1·6
Ce	<0·01	1·8	2·5	3·6	6·7	14	34	70	42	29	26	0·31
Pr	0·22	0·21	0·34	0·77	1·3	2·6	5·1	9·0	6·2	3·7	2·9	0·15
Nd	1·4	1·3	2·2	4·4	7·1	14·5	24	38	31	17	11	0·55
Sm	0·83	0·28	0·63	1·7	2·5	4·9	6·5	8·6	7·6	4·5	1·9	0·30
Eu	0·53	0·42	0·55	0·98	1·3	2·0	2·0	3·0	1·3	1·5	1·0	1·3
Gd	1·2	0·42	1·1	2·6	3·2	6·0	7·3	8·7	8·3	5·1	1·8	0·34
Tb	n.a.	0·06	0·15	n.a.	0·41	0·85	1·1	1·2	1·2	0·71	0·22	<0·01
Dy	1·0	0·32	0·97	2·6	2·9	5·7	6·8	6·9	6·5	4·3	1·1	<0·01
Ho	0·23	0·07	0·21	0·56	0·61	1·2	1·4	1·3	1·3	0·85	0·22	<0·01
Er	0·61	0·22	0·64	1·6	1·7	3·2	3·8	3·5	3·7	2·4	0·66	<0·01
Tm	0·09	0·03	0·10	0·21	0·24	0·44	0·53	0·48	0·53	0·34	0·09	0·01
Yb	0·49	0·26	0·63	1·2	1·5	2·5	3·2	2·9	3·5	2·2	0·68	<0·01
Lu	0·08	0·02	0·09	0·19	0·21	0·39	0·47	0·41	0·59	0·31	0·10	0·01
Ge	1·5	0·7	1·8	2·0	1·6	1·8	1·8	1·8	n.a.	1·8	1·1	1·5
Hf	0·3	<0·1	0·3	0·9	1·3	2·1	2·7	1·5	n.a.	0·2	<0·1	0·1
Ta	<0·1	<0·1	0·2	<0·1	0·1	0·1	0·6	3·2	1·2	0·3	0·2	<0·1

*Major and trace elements (XRF) from Ulrich (1995).
†Fe_2O_3 is total iron.
Minerals given in parenthesis are present only as pseudomorphs and their amount has been estimated on the basis of a normative mineral content. The percentage of retrograde alteration is also indicated. Alteration products are mainly amphibole on the pyroxene site and albite and clinozoisite on the plagioclase site (see Müntener *et al.*, 2000). The bulk chemical composition of the rocks was determined by X-ray fluorescence (XRF) analyses, with a sequential spectrometer (Philips PW 1404) using natural US Geological Survey (USGS) reference rock samples for calibration. The REE content of the rocks has been determined by solution ICP-MS with an ELAN 500 (Perkin–Elmer Sciex) instrument installed at EMPA Dübendorf, Switzerland. The precision of the method for multiple measured samples was ~5–20% (1σ). Accuracy of 0–20% was obtained by measuring international standards (BHVO-1; MRG-1). LOI, loss on ignition.

Spinel

Green, hercynitic spinel occurs mainly in Fe gabbros (Fig. 2b). Rare brownish dark cores display the highest Cr_2O_3 contents of ~3·5 wt % whereas the green spinel rims exhibit lower contents of ~1–1·5 wt %.

Apatite

Apatite saturation is achieved only in a few Fe gabbros and in Fe–Ti diorites. Apatite has abundant REE contents with a preferential incorporation of LREE (Fig. 6d), which may affect bulk REE although apatite is only of minor modal abundance. The bulk-rock composition of Fe gabbro B-F 107 (corresponding mineral analysis in sample B-F 103) contains apatite and has La and Ce contents about five times higher than in Fe gabbro B-F 7 without apatite. Apatite contributes significantly to the REE budget in high-P_2O_5 low-SiO_2 Fe–Ti diorites (Figs 5 and 6).

CONDITIONS OF INTRUSION

Temperature

Solvus thermometry (Wells, 1977) of coexisting clino- and orthopyroxene yields temperatures of 780–840°C for all samples. This indicates slow cooling of the gabbro and re-equilibration of Ca and Mg in pyroxenes under granulite facies conditions. In sample B-F7 the pyroxenes coexist with olivine and spinel. Calculation of the equilibrium Al-enstatite + forsterite = enstatite + spinel yields temperatures of ~1200°C for large orthopyroxenes (Müntener *et al.*, 2000), which is probably close to the solidus temperature (e.g. Green & Ringwood, 1967). Calculation of the same equilibria yields 840°C for the

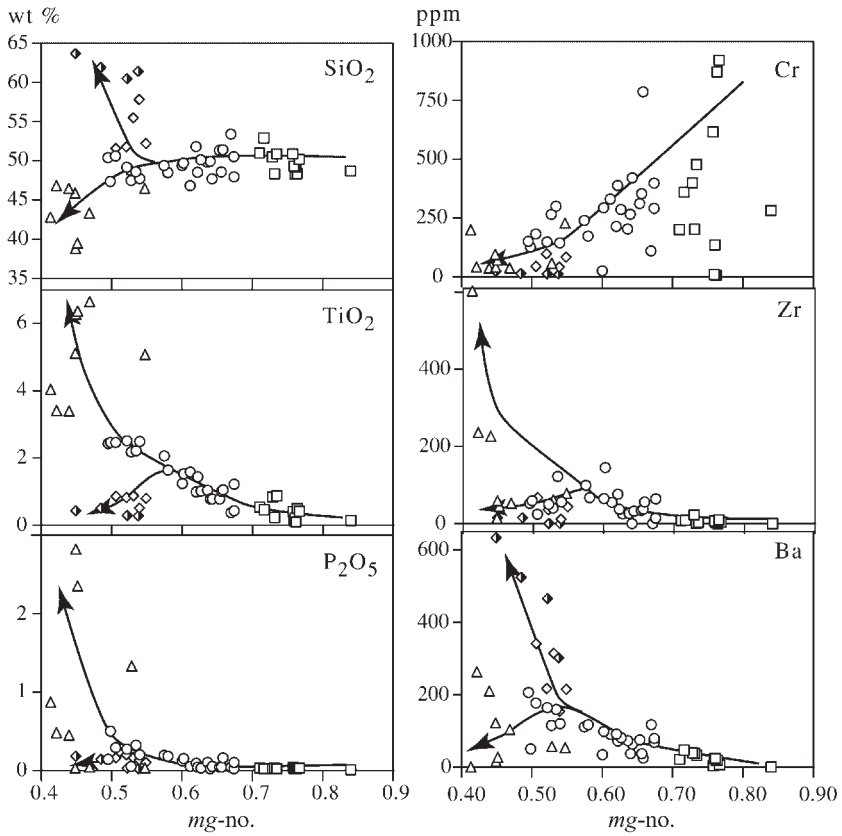

Fig. 3. Variation diagrams for major and trace elements in the Braccia gabbro with *mg*-number [= molar Mg/(Mg + Fe_{tot})]. □, Mg gabbro; ○, Fe gabbro; △, Fe–Ti diorite; ◇, opx diorite; half-filled diamonds, qtz diorite. The arrows indicate the chemical evolution from Mg to Fe gabbros. The trend is split into two branches when the diorite dykes formed.

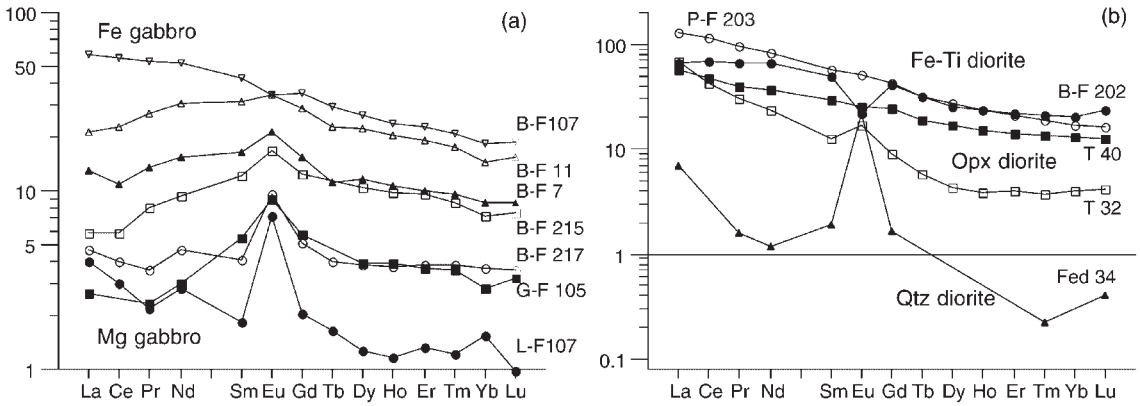

Fig. 4. REE patterns for different gabbro types (a) (Mg gabbro: L-F 107, G-F 105, B-F 217, B-F 215; Fe gabbro: B-F 7, B-F 11, B-F 107) and diorite dykes (b) (Fe–Ti diorite: B-F 202, P-F 203; opx diorite: T40, T32; qtz diorite: Fed 34). Normalization to a C1 chondrite (Sun & McDonough, 1989).

corona assemblage (Hermann, 1997; Müntener *et al.*, 2000). Additionally, the Al_2O_3 content of magmatic clinopyroxene (6·5 wt %) is significantly higher than that in spinel-corona clinopyroxene (4·1 wt %) and in garnet corona clinopyroxene (2·7 wt %). These observations suggest that aluminium in pyroxene has a significantly

Table 2: Average mineral composition of the Braccia gabbro

	Clinopyroxene					Orthopyroxene						
Sample:	G- F	G-F	B-F 7	B-F	B-F	L-F	G-F	G-F	B-F 7	B-F	B-F	B-F
Mean of:	105	101		219	103	107	105	101		219	103	115
	(9)	(15)	(14)	(18)	(26)	(24)	(14)	(8)	(16)	(8)	(19)	(11)
SiO_2 wt %	48·3	49·7	49·5	50·0	50·4	52·4	51·8	52·9	51·3	51·5	50·3	52·3
TiO_2	1·60	1·28	1·20	0·97	0·57	0·26	0·15	0·24	0·16	0·20	0·08	0·08
Al_2O_3	7·32	5·59	6·57	5·60	3·77	4·66	4·19	3·58	4·16	3·30	1·83	1·48
Cr_2O_3	0·17	0·27	0·09	<0·03	0·06	0·04	0·07	0·15	0·05	<0·03	<0·03	<0·03
FeO	6·28	5·69	7·45	8·37	11·2	14·1	16·3	14·5	20·1	21·7	29·3	23·1
MnO	0·15	0·16	0·18	0·23	0·26	0·30	0·33	0·35	0·40	0·47	0·63	0·70
NiO	0·03	<0·03	0·03	n.a.	n.a.							
MgO	13·1	14·0	12·6	12·5	11·4	27·5	26·2	27·6	23·2	22·0	17·2	21·7
CaO	21·9	22·4	21·4	21·3	21·6	0·73	0·80	0·66	0·52	0·78	0·61	0·60
Na_2O	1·10	0·87	1·07	1·08	0·69	0·03	0·09	0·04	0·04	0·04	<0·03	0·05
K_2O	<0·03	<0·03	<0·03	<0·03	<0·03	<0·03	<0·03	<0·03	<0·03	<0·03	<0·03	<0·03
Σ	100·0	100·0	100·0	100·0	100·0	100·0	100·0	100·0	100·0	100·0	100·0	100·0
mg-no.	0·79	0·81	0·75	0·73	0·65	0·78	0·74	0·77	0·67	0·64	0·51	0·63

	Plagioclase							Olivine		Spinel
Sample:	L-F	G-F	B-F 7	B-F	B-F	P-F	B-F	L-F	B-F 7	B-F 7
Mean of:	107	105		219	103	203	115	107		
	(2)	(13)	(24)	(14)	(4)	(3)	(4)	(30)	(10)	(23)
SiO_2 wt %	53·6	54·4	55·4	58·3	57·3	57·2	58·6	38·4	37·5	0·08
TiO_2	<0·02	0·04	0·03	<0·02	0·03	<0·02	<0·02	<0·02	<0·02	0·03
Al_2O_3	29·5	28·8	28·1	26·4	26·7	25·6	26·2	<0·03	<0·03	60·3
Cr_2O_3	<0·03	<0·03	<0·03	<0·03	<0·03	<0·03	<0·03	<0·03	<0·03	0·93
Fe_2O_3	0·13	0·16	0·14	0·22	0·28	2·33	0·03	0·00	0·00	2·36
FeO	0·00	0·00	0·00	0·03	0·00	0·00	0·02	21·1	24·6	26·7
MnO	<0·04	<0·04	<0·04	<0·04	<0·04	<0·04	<0·04	0·26	0·37	0·09
NiO	n.a.	n.a.	n.a.	n.a.	n.a.	n.a.	n.a.	0·08	0·04	0·08
MgO	<0·02	0·03	0·02	0·03	0·06	<0·02	0·02	40·15	37·48	9·59
CaO	11·6	11·0	10·4	7·36	8·52	7·55	7·90	<0·02	<0·02	<0·02
Na_2O	5·07	5·53	5·92	7·28	6·51	7·22	7·08	<0·03	<0·03	0·05
K_2O	<0·03	0·10	0·05	0·31	0·57	0·07	0·18	<0·03	<0·03	<0·03
Σ	100·0	100·0	100·0	100·0	100·0	100·0	100·0	100·0	100·0	100·2
An	0·56	0·52	0·49	0·36	0·42	0·37	0·38			
mg-no.								0·77	0·73	0·37

higher closure temperature than two-pyroxene solvus thermometry and that equilibration temperatures probably exceeded 1000°C (Hermann, 1997).

Pressure

Age determinations have shown that partial melting and concomitant granulite facies equilibration in the continental crust are caused by the gabbro intrusion (Hansmann *et al.*, 1996; Hermann *et al.*, 1997). Therefore, the pressure of 1·0 GPa calculated from granulite facies assemblages in the pelitic lower crust is also valid for the gabbro. This is consistent with the observed assemblage of magmatic minerals in sample B-F7 with pl + cpx + opx + spl ± ol, which indicates subsolidus cooling at

	Ti-pargasite						Ilmenite					
Sample:	L-F	G-F	G-F	B-F7	B-F	P-F	G-F	B-F 7	B-F	B-F	P-F	B-F
Mean of:	107	101	105		219	203	105		219	103	203	115
	(11)	(9)	(9)	(18)	(21)	(23)	(8)	(4)	(8)	(1)	(5)	(1)
SiO_2 wt %	40·9	41·3	39·9	40·4	40·1	41·9	<0·06	0·21	<0·06	<0·06	<0·06	<0·06
TiO_2	4·08	3·64	5·70	5·75	4·40	2·19	52·9	51·4	51·8	52·2	52·2	52·4
Al_2O_3	14·8	14·6	14·2	13·9	14·6	12·4	0·03	0·04	0·03	<0·03	0·03	<0·06
Cr_2O_3	0·03	0·19	0·25	0·09	<0·03	<0·03	0·06	0·14	0·03	0·04	<0·03	<0·03
Fe_2O_3	2·36	0·32	1·22	0·11	0·38	5·28	0·17	3·27	2·16	1·32	0·93	0·70
FeO	5·5	9·3	10·4	12·0	13·0	13·6	44·7	43·0	44·8	45·5	45·1	45·1
MnO	0·09	0·04	0·13	0·07	0·10	0·21	1·66	0·37	0·35	0·54	1·55	1·53
NiO	<0·03	0·04	0·04	<0·03	n.a.	n.a.	n.a.	n.a.	n.a.	n.a.	n.a.	n.a.
MgO	14·9	13·1	11·8	10·7	10·4	8·76	0·33	1·59	0·77	0·36	0·12	0·22
CaO	12·0	11·9	11·9	11·7	11·4	11·3	0·04	<0·02	<0·02	<0·02	<0·02	<0·02
Na_2O	2·25	2·06	1·85	1·48	2·01	1·01	0·07	0·06	<0·03	0·04	<0·03	<0·03
K_2O	1·13	1·52	0·83	2·26	1·71	1·41	<0·03	<0·03	<0·03	<0·03	<0·03	<0·03
H_2O	1·99	2·00	1·93	1·62	1·93	2·00						
Σ	100·0	100·0	100·0	100·0	100·0	100·0	100·0	100·0	100·0	100·0	100·0	100·0
mg-no.	0·78	0·71	0·65	0·61	0·58	0·46	0·01	0·06	0·03	0·01	0·00	0·01
edenite	0·69	0·73	0·56	0·72	0·73	0·37						
plagioclase	0·15	0·14	0·13	0·14	0·18	0·19						
Tschermaks	1·56	1·37	1·70	1·41	1·48	1·54						
Fe^{3+}/ Fe(tot)	0·28	0·03	0·10	0·01	0·03	0·26						

Sample G-F 101 is an olivine Mg gabbro (all olivine altered) that has pyroxenes with the highest *mg*-number. The mode is intermediate between G-F 105 and L-F 107. Sample B-F 219 is the freshest ilmenite-rich Fe gabbro. It contains ~5% Ti-pargasite. Sample B-F 103 is a Fe gabbro and was collected near sample B-F 107 from the same lithotype. Mineral compositions were determined using a Cameca SX-50 electron microprobe. The acceleration potential was 15 kV and the beam current was 20 nA with a beam size of ~1 μm. *mg*-number refers to molar Mg/(Mg + Fe_{tot}) ratio. Ferric iron and exchange vectors starting from tremolite have been calculated for amphiboles using Σ(cat) − K − Na − Ca = 13 and 46 charges.

~1·0 GPa (Green & Ringwood, 1967). Further evidence for gabbro crystallization above 0·8 GPa stems from experimental evidence on dry basaltic systems that crystallization of clinopyroxene precedes that of plagioclase (Green & Ringwood, 1967; Elthon & Scarfe, 1984), which fits the observation of abundant pyroxenite cumulates in the gabbro.

DISCUSSION

In situ differentiation of the Braccia gabbro

There are several observations indicating a magmatic evolution of the Braccia gabbro. A rough subdivision into different gabbros and diorites is possible on the basis of field relations, the increase in accessory minerals and the continuous increase of the *mg*-number in whole-rock analyses (Table 1). A more detailed insight into differentiation is provided by whole-rock incompatible elements (Fig. 3), and especially the increase of REE (Fig. 4). Through much of the gabbro evolution the modal abundance of pyroxenes and plagioclase remains roughly constant (Table 1) whereas the concentrations of incompatible trace elements change drastically (Fig. 3). This is a typical feature of *in situ* crystallization as defined by Langmuir (1989). The major element composition of a gabbro–norite cumulate is close to the composition of the liquid from which it crystallized. Thus, major element concentration, and consequently the mode, remains constant during differentiation

Table 3: Trace element compositions of minerals determined with laser-ablation microprobe ICP-MS

	G-F 105 Mg gabbro					G-F 101 Mg gabbro			B-F 7 Fe gabbro				B-F 219 Fe gabbro				
Min.:	Cpx	Opx	Plag	Parg	Ilm	Cpx	Opx	Parg	Cpx	Opx	Plag	Ilm	Cpx	Opx	Plag	Parg	Ilm
Mean:	(6)*	(5)	(3)	(2)*	(2)*	(5)	(4)	(4)	(2)	(4)	(4)	(3)	(3)	(3)	(4)	(2)	(3)
Sc	n.a.	49	19	n.a.	n.a.	104	43	84	59	58	12	6·4	168	57	2·1	132	36
V	626	311	1·8	1060	296	565	214	877	445	254	1·1	762	718	298	3·3	1185	1417
Cr	n.a.	565	8·2	n.a.	n.a.	1747	910	2173	412	297	3·8	270	<6·2	<6·0	<12	4·2	9·9
Ni	n.a.	217	2·3	n.a.	n.a.	91	150	289	66	104	0·78	799	25	36	1·5	56	101
Zn	44	164	<1·55	65	48	53	179	155	44	202	2·7	347	72	262	6·4	92	123
Ga	n.a.	9·4	19	n.a.	n.a.	11	8·1	25	15	13	23	0·31	13	10	37	45	1·3
Rb	<0·15	<0·05	0·19	1·4	<0·14	0·06	0·06	12	0·08	0·16	<0·03	0·16	0·03	0·02	0·36	7·9	<0·01
Sr	16	0·24	540	113	2·7	19	0·53	120	38	0·57	348	4·7	20	0·35	555	133	4·8
Y	14	1·1	0·14	24	0·25	25	1·5	47	53	4·9	0·28	0·35	47	3·9	0·21	58	0·52
Zr	12	0·85	0·12	10	0·66	38	1·8	33	104	7·6	0·07	14	82	6·0	<0·03	80	1·9
Nb	<0·14	<0·01	<0·01	<0·22	0·37	0·17	0·02	17	0·07	<0·01	<0·01	62	0·07	<0·01	<0·03	7·5	27·5
Ba	10	<0·11	51	74	<0·24	0·38	0·52	143	11	0·59	98	0·26	0·38	0·07	155	239	<0·02
La	0·29	<0·01	0·38	0·55	<0·03	1·4	0·05	2·8	2·7	0·04	2·9	0·1	2·9	0·03	2·7	6·5	0·24
Ce	1·4	0·02	0·63	2·5	<0·02	6·1	0·15	12	14	0·09	5·1	0·21	12	0·11	3·8	24	0·37
Pr	0·36	<0·03	0·07	0·56	<0·03	1·2	0·02	2·5	3·0	0·02	0·51	0·02	2·5	0·02	0·34	4·5	0·05
Nd	2·6	0·02	0·3	4·5	<0·13	7·4	0·13	15·	20	0·10	1·8	0·08	16	0·15	1·1	25	0·48
Sm	1·3	0·01	0·05	2·3	<0·14	3·1	0·07	5·7	7·6	0·08	0·26	0·01	6·2	0·13	0·15	8·8	0·11
Eu	0·62	0·01	0·22	1·1	<0·03	1·1	0·02	2·2	1·7	0·03	0·85	0·01	1·9	0·05	1·1	3·5	0·04
Gd	2·0	0·04	0·05	3·7	<0·22	3·9	0·07	7·1	7·7	0·17	0·16	0·01	7·4	0·22	0·24	9·9	0·05
Tb	0·43	0·01	<0·01	0·63	<0·03	0·79	0·03	1·3	1·7	0·06	0·02	<0·01	1·4	0·06	0·01	1·8	0·01
Dy	2·8	0·14	<0·01	4·4	<0·11	5·3	0·19	9·0	11	0·59	0·08	0·01	9·6	0·54	0·03	12	0·04
Ho	0·60	0·04	<0·01	1·0	<0·04	1·1	0·05	1·8	2·2	0·19	0·01	<0·01	2·0	0·18	<0·01	2·3	<0·01
Er	1·5	0·16	<0·01	2·5	<0·1	3·0	0·22	5·1	6·2	0·82	0·03	<0·01	5·5	0·62	<0·02	6·4	0·02
Tm	0·21	0·04	<0·01	0·34	<0·04	0·40	0·05	0·69	0·91	0·16	<0·01	<0·01	0·74	0·12	<0·01	0·88	<0·01
Yb	1·40	0·29	<0·01	2·1	<0·16	2·5	0·37	4·1	5·5	1·3	<0·01	0·01	4·8	0·87	0·03	5·3	0·02
Lu	0·19	0·05	<0·01	0·33	<0·02	0·39	0·08	0·62	0·83	0·25	<0·01	<0·01	0·70	0·18	<0·01	0·70	<0·01
Hf	n.a.	n.a.	n.a.	n.a.	n.a.	n.a.	n.a.	n.a.	n.a.	n.a.	n.a.	n.a.	3·4	0·29	<0·03	3·4	0·06
Ta	<0·04	<0·01	<0·01	<0·05	0·09	0·04	<0·01	0·54	0·03	<0·01	<0·01	6·2	0·02	<0·01	<0·01	0·43	2·7
Pb	0·63	<0·15	0·36	0·56	<0·16	<0·25	<0·12	<0·40	0·35	<0·15	2·1	<0·13	0·13	<0·08	1·63	0·80	0·03
Th	<0·04	n.a.	n.a.	<0·05	<0·05	n.a.	n.a.	n.a.	n.a.	n.a.	n.a.	n.a.	0·03	<0·02	<0·02	0·04	<0·02
U	<0·03	n.a.	n.a.	<0·05	<0·03	n.a.	n.a.	n.a.	n.a.	n.a.	n.a.	n.a.	<0·02	<0·02	<0·02	<0·02	<0·02

whereas the incompatible trace elements increase with increasing formation of cumulates. According to Langmuir (1989), gabbros most probably form in a solidification zone with an unknown proportion of cumulates and interstitial liquids.

The Mg gabbros display an accentuated positive Eu anomaly, which indicates the presence of cumulus plagioclase. It is much more difficult to prove the presence of interstitial liquid because the gabbros cooled slowly. There is no zoning observable in major, minor and trace elements in minerals of the gabbro. Late crystallizing Ti-pargasite displays a constant partitioning to early crystallizing pyroxenes (Figs 5b and 7a). These observations indicate that the minerals equilibrated with possible interstitial liquid. Crystallization of new phases in subsolidus conditions such as garnet would lead to a significant redistribution of major and trace elements during cooling. In the Braccia gabbro, the subsolidus cooling to 800°C did not lead to a change in paragenesis (Müntener *et al.*, 2000) preventing subsolidus redistribution of REE as a result of changing phases. The Al content of magmatic pyroxenes is significantly higher than that of the corona pyroxenes, indicating that Al reequilibration ceased before coronas were formed. The REE are probably incorporated in pyroxenes by an exchange $REE^{(VI)}Al^{(IV)}Ca_{-1}Si_{-1}$ (Schosnig & Hoffer, 1998) and thus it is likely that, similar to Al, the REE contents of minerals did not change below ~1000°C. Therefore the problem to solve is to estimate the amount of cumulus phases and interstitial liquid from a rock that did not

	B-F 103 Fe gabbro					P-F 203 Fe–Ti diorite			
Min.:	Cpx	Opx	Plag	Ilm	Apa	Plag	Parg	Ilm	Apa
Mean:	(3)	(3)	(3)	(2)	(2)	(3)	(5)*	(2)	(2)
Sc	188	56	1·9	30	2·7	2·9	90	3·0	2·0
V	519	204	<0·73	243	2·1	21	956	253	6·0
Cr	309	160	<12	350	<24	<10·0	27	8·4	<5·8
Ni	61	90	2·2	127	<2·2	0·92	26	91	3·7
Zn	157	521	8·9	286	<2·1	4·5	298	118	4·3
Ga	11	8·7	48	0·48	1·0	46	75	0·13	0·45
Rb	0·07	0·04	2·3	0·02	0·09	1·7	7·8	0·01	0·07
Sr	15	0·45	421	4·5	197	1477	123	5·0	750
Y	144	12	0·49	1·0	706	4·1	94	0·59	181
Zr	353	13	0·05	1·6	9·9	0·35	33	6·9	0·70
Nb	0·02	0·02	<0·02	200	<0·04	1·6	32	403	5·6
Ba	0·24	0·45	199	0·24	1·5	116	308	0·12	1·5
La	16	0·33	15	0·29	578	13	48	0·2	165
Ce	69	1·7	21	0·75	1800	16	142	0·68	408
Pr	14	0·23	1·8	0·09	246	1·2	21	0·09	50
Nd	75	1·1	5·3	0·40	1014	3·9	97	0·39	246
Sm	25	0·41	0·59	0·09	210	0·62	24	0·07	48
Eu	2·7	0·06	2·2	0·04	16	2·5	5·3	0·02	9·4
Gd	25	0·62	0·69	0·12	213	0·84	22	0·05	50
Tb	4·8	0·18	0·03	0·02	29	0·11	3·5	0·01	6·9
Dy	30	1·6	0·13	0·13	150	0·74	20	0·03	36
Ho	5·9	0·43	0·02	0·03	28	0·15	3·7	0·01	6·6
Er	17	1·7	0·04	0·08	69	0·40	10	0·03	18
Tm	2·3	0·34	<0·01	0·02	8·0	0·05	1·3	0·01	2·1
Yb	15	3·0	<0·01	0·14	42	0·31	7·6	0·06	11
Lu	2·1	0·54	<0·01	0·02	5·8	0·04	1·1	0·02	1·9
Hf	11	0·55	<0·01	0·16	0·06	0·03	4·1	0·54	0·03
Ta	0·02	<0·01	<0·01	16	0·02	0·09	1·5	29	0·21
Pb	0·51	0·10	8·8	<0·09	1·6	18	7·6	0·13	2·3
Th	0·71	0·16	<0·02	0·05	113	0·07	0·95	0·03	15
U	0·06	0·02	<0·02	0·02	35	0·05	0·18	0·04	12

*Measured with argon carrier gas.
A 193 nm excimer laser in combination with an ELAN 6000 ICP-Mass Spectrometer have been used for *in situ* trace element determinations in the different mineral phases. Details of the LAM-ICP-MS system have been described by Günther *et al.* (1997). An Ar–He mix has been used as carrier gas. The data reduction procedure, the quantification, and the determination of the limits of detection have been described by Longerich *et al.* (1996). The trace element concentrations have been compared with ICP-MS solution data and show a variation in the range of 5–15% between the two methods. The precision determined from five replicates on an amphibole sample was better than 3–10% for most of the isotopes. Similar experiments on the NIST 612 glass reference material led to 2–5% RSD. n.a., not analysed.

change mineralogy but equilibrated at subsolidus conditions. In the next section we show an approach to estimate these proportions for the measured samples by mineral REE modelling.

REE modelling of *in situ* differentiation

The strategy of the proposed model is to calculate mineral REE patterns starting from a primitive gabbro liquid. The most important variables of *in situ* crystallization are the degree of differentiation F and the amount of interstitial liquid L (both given in percent). As the minerals do not show any zoning, the trapped interstitial liquid completely equilibrated with the existing cumulus phases. For every sample we calculated a best fit to the measured patterns. In this way we can obtain information about the degree of differentiation for the sample. Additionally, it helps to decide if the gabbro represents a pure cumulate

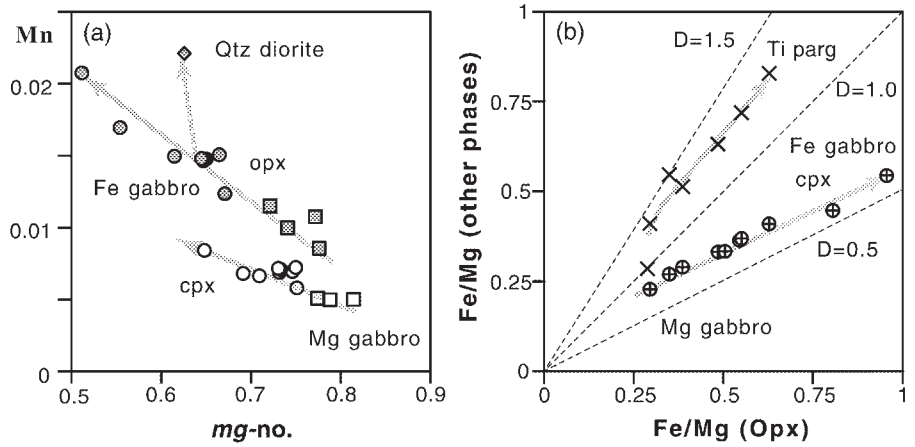

Fig. 5. (a) Change of clino- and orthopyroxene composition with changing *mg*-number. Squares, Mg gabbro; circles, Fe gabbro; diamonds, qtz diorite. (b) Fe–Mg partitioning between orthopyroxene and coexisting phases based on average mineral compositions of the respective samples.

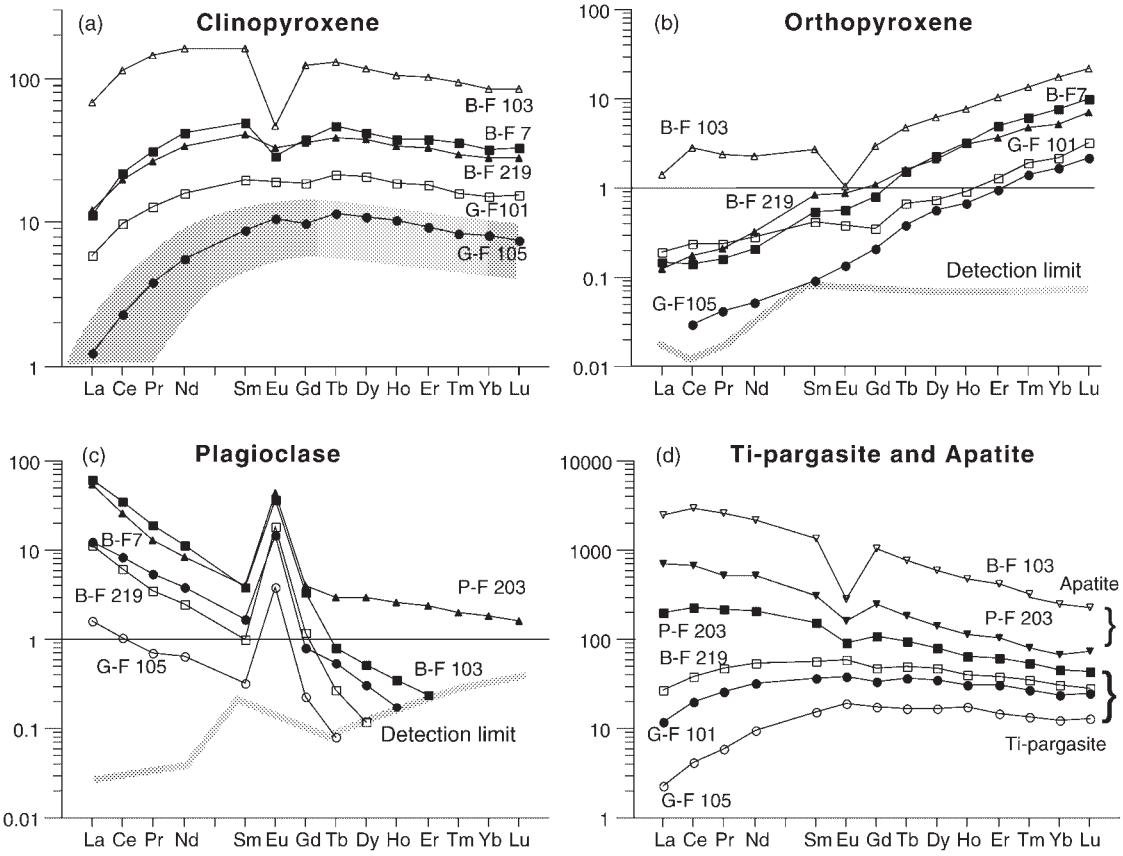

Fig. 6. REE patterns for magmatic minerals normalized to a C1 chondrite (Sun & McDonough, 1989). For minerals with low REE contents the detection limit is indicated (grey line). The compositions of clinopyroxene from gabbros of the Oman ophiolite (Kelemen *et al.*, 1997) are shown for comparison (grey field).

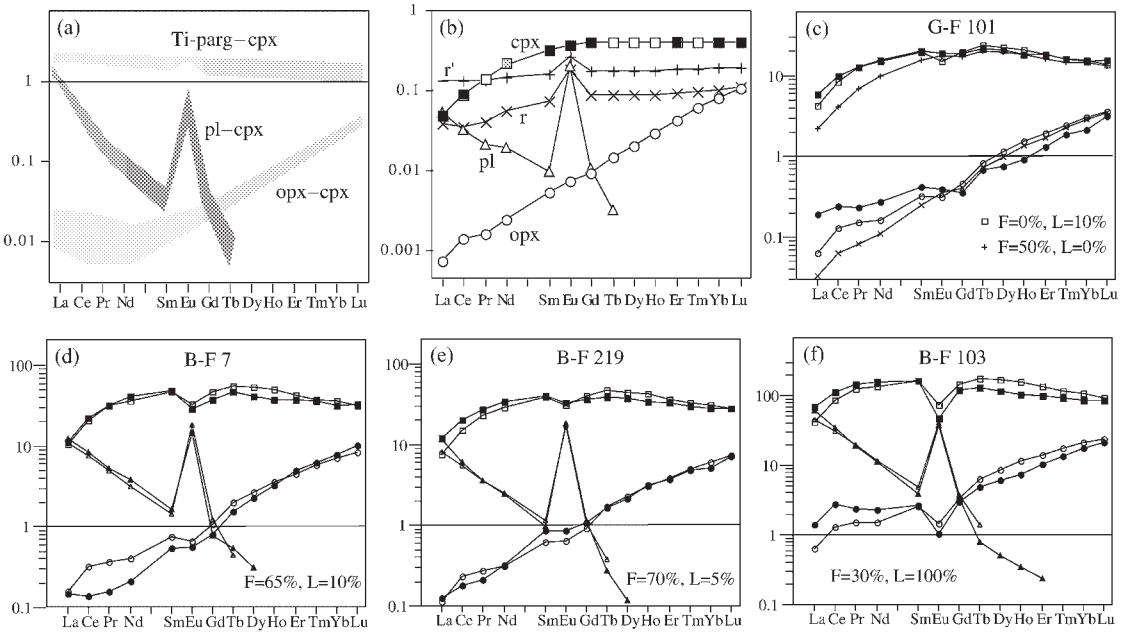

Fig. 7. (a) Range of partitioning for different mineral–clinopyroxene pairs. (b) Mineral- and bulk-rock–melt partitioning used for the model. Cpx–melt values (■) are based on the experiments of Hauri *et al.* (1994). The K_d values used are: La, 0·05; Ce, 0·09; Pr, 0·14; Nd, 0·22; Sm, 0·33; Eu, 0·37; Gd–Lu, 0·41. Pl–melt and Opx–melt are calculated from mineral partitioning shown in (a). r refers to bulk-rock partitioning without trapped liquid whereas r′ corresponds to a partitioning with 10% of trapped liquid (see also Table 4). (c–f) REE patterns normalized to C1 chondrite (Sun & McDonough, 1989). Comparison between measured (black filled) and modelled (grey or white) REE contents of minerals. Squares, clinopyroxene; circles, orthopyroxene; triangles, plagioclase. *F*, degree of differentiation with respect to primitive gabbro G-F 105; *L*, fraction of trapped liquid. (See text for discussion.)

($L = 0\%$) or a crystallized liquid ($L = 100\%$) or something between these. The model cannot be applied to the diorites because they contain significant amounts of apatite and Ti-pargasite, which strongly influence the REE budget. Nevertheless, the model explains observed first-order changes in mineral REE patterns of the gabbro. Details of the model are explained in Table 4 and Fig. 7a and b, and the results are shown in Fig. 7c–f.

Results

Sample G-F 101 displays higher amounts of REE and a significant enrichment of LREE with respect to sample G-F 105. If the enrichment is modelled without interstitial liquid ($L = 0$) the degree of differentiation has to be $F = 50\%$ to explain the HREE enrichment. However, there is no way to explain the LREE enrichment (Fig. 7c). With 10% of trapped liquid and $F = 0$ the calculated patterns are very similar to the measured ones. This example shows that trapped liquid has strongest influence on the LREE content in pyroxenes because of the very low pyroxene–melt K_d values (Fig. 7b). The presence of interstitial liquid is supported by the *mg*-number of pyroxenes. If differentiation had been 50% the *mg*-number of pyroxenes from sample G-F 101 should be significantly lower than that of sample G-F105. In contrast, the opposite feature has been observed, supporting the enrichment of incompatible trace elements by trapped liquids. Thus the higher amount of trace elements in G-F 101 with respect to G-F 105 at the same *mg*-number of pyroxenes is a good example to illustrate the effect of trapped liquid.

The mineral patterns of samples B-F 7 and B-F 219 are very similar (Fig. 5). However, clinopyroxene B-F 7 displays a more pronounced negative Eu anomaly, which resulted in a slightly different fit. B-F 7 is best modelled by $F = 65\%$ and $L = 10\%$ (Fig. 7d) whereas B-F 219 fits best with $F = 70\%$ and $L = 5\%$ (Fig. 7e). This part of the modelling shows that a similar REE enrichment of ~10 times with respect to G-F 105 can be achieved by different degrees of differentiation and trapped liquid, respectively. However, a higher amount of trapped liquid results in a more accentuated negative Eu anomaly in pyroxenes. Trapped liquid in highly differentiated gabbros has a negative Eu anomaly because of previous plagioclase fractionation. Consequently, whole-rock analyses with trapped liquid, as for example B-F 7, have a smaller negative Eu anomaly than 'pure' cumulates. REE modelling is consistent with the lower *mg*-number of pyroxenes in sample BF 219 with respect to sample B-F7. Barnes (1986) demonstrated that in gabbro norites

Table 4: REE-modelling for in situ *differentiation with complete equilibration of cumulus phases and interstital melt*

(I) *Parameters*

(1) $D_{Cpx/M}$: ⇒ calculation of $D_{Opx/M}$, $D_{Pl/M}$

(2) Starting liquid $L_0 = REE_{Cpx}^{G\text{-}F\ 105} D_{Cpx/M}$

(3) $D_{rock/M} = 0{\cdot}2D_{Cpx/M} + 0{\cdot}25D_{Opx/M} + 0{\cdot}55D_{Pl/M}$

(4) $D'_{rock/M} = 0{\cdot}9D_{rock/M} + 0{\cdot}1$ (10% interstitial liquid)

(II) *Variables*

(5) Degree of differentiation, F (range 0–1)

(6) Fraction of interstitial liquid, L (range 0–1)

(III) *Calculations*

(7) REE_{rock} = cumulus + interstitial melt

$= L_0(1-F)^{(1-D'rock/M)}[D_{rock/M}(1-L)+L]$

(8) $REE_{rock} = 0{\cdot}2REE_{Cpx} + 0{\cdot}25REE_{Opx} + 0{\cdot}55REE_{Pl}$

and $REE_{Opx}/REE_{Cpx} = D_{Opx/M}/D_{Cpx/M}$ = const.

and $REE_{Pl}/REE_{Cpx} = D_{Pl/M}/D_{Cpx/M}$ = const.

⇒ REE_{Cpx}, REE_{Opx}, REE_{Pl}

(1) We used a cpx–melt partition coefficient (Fig. 7b) based on the experiments of Hauri *et al.* (1994), which was determined in a bulk composition similar to the Braccia gabbro and with a clinopyroxene that had a 9·2 wt % Al_2O_3 content. From the measured mineral–mineral K_d values (Fig. 7a) the partitioning opx–melt and plag–melt has been calculated (Fig. 7b). (2) The starting liquid (L_0) was calculated from cpx G-F 105, which has a high *mg*-number, the lowest REE contents and a smooth pattern (Fig. 6). (3) The bulk $D_{rock/melt}$ was calculated using the average modal abundances of plagioclase (55%), orthopyroxene (25%) and clinopyroxene (20%). (4) To calculate the enrichment of elements in the residual melt by Rayleigh fractionation [see step (7)] a $D'_{rock/melt}$ has been used that takes into account that an assumed average of ~10% melt is trapped during differentiation. Trial and error calculations with different D values showed that the model is much less sensitive to different D' values than to variations in F and L. (5, 6) The main variables in the model are the unknowns of the *in situ* crystallization (F and L). (7) The whole-rock REE content is determined by two components: (a) the proportions of cumulus phases ($1 - L$) crystallizing from a melt with the given $D_{rock/M}$ after F% of differentiation with respect to the formation of the gabbro G-F 105 has been calculated using Rayleigh fractionation; (b) the amount (L) of the same liquid trapped in the cumulates. (8) The REE contents of cpx, opx and plag can be calculated using the given three equations.

~10% of trapped liquid leads to a shift in *mg*-number of ~0·03. Thus, the *mg*-number is much less affected by trapped liquid than the REE composition.

The pyroxenes of sample B-F 103 display a strong negative Eu anomaly and, in particular, the orthopyroxene has strongly enriched LREE, both indicating significant presence of trapped liquid. In fact, the best fit of the patterns was achieved if the sample represents a fully crystallized liquid (L = 100%) after 30% of differentiation (Fig. 7f). This sample already has accessory apatite and the model reaches its limitations. More complex calculations involving apatite for this sample have shown that it is best explained by a crystallized liquid. The very low *mg*-number of B-F 103 pyroxenes (Table 3) supports the interpretation of a crystallized liquid.

LILE such as Ba provide independent constraints on the proposed proportions of cumulates and interstitial liquid derived from REE modelling. The observed enrichment of Ba in plagioclase (Table 4) for samples B-F7 and B-F 103 can be reproduced using a K_d Ba–melt of 0·5 for An_{50} plagioclase (Bindeman *et al.*, 1998). In sample B-F 219 it is more difficult to calculate the Ba content of plagioclase because of the presence of Ba-rich Ti-pargasite. However, it seems that the measured Ba concentration in plagioclase in sample B-F 219 is higher than calculated from the model.

Implications of modelling

(1) The measured REE patterns can successfully be modelled by *in situ* differentiation. The modelling shows that some gabbros are nearly pure cumulates whereas others represent frozen liquids.

(2) In cumulates with <10% trapped liquid the *mg*-number of pyroxenes permits us to estimate the degree of differentiation. In contrast, the amount and especially REE ratios in minerals are strongly dependent on and allow us to estimate the amount of trapped liquid.

(3) The observed accentuated negative Eu anomaly in some of the pyroxenes does not indicate a strong negative Eu anomaly in the parental melt. It originates rather from high amount of trapped liquid, as pointed out by Cawthorn (1996).

(4) Gabbros representing liquid compositions are very similar to highly differentiated gabbro cumulates with low-*mg*-number pyroxenes and high amounts of incompatible trace elements. However, frozen liquids can be recognized by a slightly negative Eu anomaly in whole-rock analyses and by an accentuated negative Eu anomaly in the pyroxenes.

(5) Highly incompatible elements such as LREE, Nb, Ta and P have to be incorporated in minerals when trapped liquids crystallize. It is suggested that this leads to formation of apatite (P, LREE) and ilmenite (Nb, Ta) in the gabbros. This is supported by the observation that traces of apatite and high concentrations of Nb and Ta in ilmenite formed in sample B-F 103 (30% F, 100% L), whereas apatite is absent and ilmenite with moderate Nb and Ta concentration is present in sample B-F 219 (70% F, 5% L). Thus accessory minerals are an ambiguous indicator of differentiation.

Highly evolved diorites

The quartz diorite and Fe–Ti diorite occur as dykes and small bodies (Fig. 1). They display contrasting chemical characteristics, with LILE strongly enriched in the SiO_2-rich quartz diorite and the HFSE and REE in the SiO_2-poor Fe–Ti diorite (Figs 5 and 6). Field evidence of dykes closely associated with Fe gabbros and the similar chemistry of Fe–Ti diorites and Fe gabbros indicate a cogenetic origin rather than crystallization from a genetically unrelated, later melt batch. This is supported by U–Pb analyses of zircons from a Fe gabbro and a Fe–Ti diorite dyke that display the same features and argue for a same crystallization age.

Ulrich & Borsien (1996) proposed that these opposite chemical signatures in the diorites are caused by immiscible liquids at a high degree of differentiation. Alternatively, these features might be due to mixing of the mafic magma with a trace-element-enriched crustal partial melt, as proposed for some rocks of the Ivrea mafic suite on the basis of isotopic studies (Voshage *et al.*, 1990; Mazzuchelli *et al.*, 1992*a*; Sinigoi *et al.*, 1994). Isotopic studies in the Braccia gabbro complex are needed to clarify the origin of the diorites.

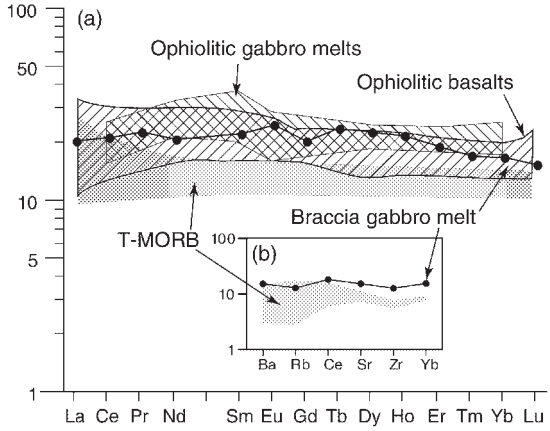

Fig. 8. (a) The REE pattern of the parental melt for the Braccia gabbro is very similar to patterns of transitional MORBs (Sun *et al.*, 1979). The calculated REE patterns of melts from ophiolitic gabbros (Piccardo, 1995) and the range of REE from basalts from Alpine ophiolites (Venturelli *et al.*, 1981) overlap with the parental Braccia gabbro melt. REE patterns normalized to C1 chondrite (Sun & McDonough, 1989). (b) LILE composition of the parental melt calculated from plagioclase composition of sample G-F 105 and K_d values at An_{50} (Ba, 0·5; Rb, 0·05; Sr, 2·7) taken from Bindeman *et al.* (1998). Zr is recalculated from clinopyroxene composition G-F 105 and K_d of 0·16 from Hauri *et al.* (1994). Normalization values from Thompson *et al.* (1984)

Composition of parental melt

The REE composition of the parental melt (see Fig. 8) can be estimated from primitive clinopyroxene. The modelling has shown that it is more important to choose a sample with no trapped liquid than the one with the highest *mg*-number because even small amounts of trapped liquid significantly influence the REE contents of clinopyroxene. G-F 105 was sampled from one of the few outcrops of the Braccia gabbro with a magmatic layering typical for gabbro cumulates. Additionally, the pyroxene pattern displays no Eu anomaly and no LREE enrichment, supporting a 'pure' cumulitic origin of the gabbro.

To calculate the REE composition of the parental melt, it is necessary to estimate the volume and composition of rocks crystallizing before G-F 105. In the most primitive gabbros found, the *mg*-number of pyroxene and olivine is ~0·8. Gabbros crystallizing from a primary mantle melt should first crystallize olivine with *mg*-number of 0·9 and should have high Cr and Ni contents. Such dunitic cumulates are not observed in the Braccia gabbro and therefore we conclude that ~10–15% of olivine and possibly some Cr-rich spinel fractionated from the melt before crystallization of the Braccia gabbro. This is important because the gabbro intruded at the crust–mantle boundary. It indicates that the primary melt started to crystallize either in a laterally situated magma chamber or even below the crust–mantle boundary. However, owing to the highly incompatible behaviour of REE in olivine and spinel, formation of ultramafic cumulates led to a proportional increase but not to a fractionation of REE in the residual liquid. Whole-rock as well as mineral analyses indicate that G-F 105 is probably not the most primitive gabbro. Thus, the recalculation of the parental melt was achieved in two steps: (1) the melt from which gabbro G-F 105 originated was calculated using the cpx–melt partitioning shown in Fig. 7b; (2) the parental melt was estimated assuming that 10% of dunite cumulates and 10% of gabbro norite were crystallized before G-F 105, based on the *mg*-number of ~0·8 in this sample.

The resulting REE pattern of the parental melt with $La_N/Yb_N = 1·2$ is characteristic for a tholeiitic melt (Fig. 8) similar to transitional mid-ocean ridge basalts (MORBs), in which La_N/Yb_N is in the range of 0·8–2 (Sun *et al.*, 1979). The inferred REE composition of the parental melt from the Braccia gabbro overlaps with those reported from ophiolitic gabbros (Piccardo, 1995; Tribuzio *et al.*, 1999*b*) and lies within the range of typical Alpine ophiolitic basalts that represent MORB melts (Venturelli *et al.*, 1981; Puschnig, 1998). The striking chemical similarity to ophiolitic gabbros is further supported by nearly identical clinopyroxene REE patterns from the Mg gabbro and from ophiolitic Oman gabbros (Kelemen *et al.*, 1997, Fig. 6). Although the Braccia gabbro intruded at the base of the continental crust, in terms of REE geochemistry it is very similar to tholeiitic gabbros emplaced in the oceanic crust. The Ba, Rb and

Sr content of the parental melt (Fig. 8b) has been recalculated using the measured plagioclase composition of sample G-F 105 and K_d values for An_{50} according to Bindeman *et al.* (1998). The Ba and Rb values are situated at the top end of the transitional MORB range (Fig. 8b) trending towards plume-type MORB compositions. The trace element characteristics of the parental Braccia gabbro melt indicate that mid-ocean-ridge-like mafic melts are not necessarily restricted to oceanic settings.

Tectonic implications

The magmatic evolution of the Braccia gabbro has important implications for the tectonic environment in Permian time in the northern part of the African plate (Fig. 9). The mafic underplating of the Braccia gabbro added at least 1 km of mafic rocks to the pre-existing continental crust (Fig. 1). The amount of Permian mafic underplating is much larger in the Ivrea Zone, situated ~150 km to the west, where locally up to 8 km of gabbros are exposed (Rivalenti *et al.*, 1981). Another gabbro complex east of Val Malenco, the Sondalo gabbro, intruded in mid-crustal levels (Tribuzio *et al.*, 1999*a*), indicating that mafic intrusions were not restricted to the lower crust (Fig. 9). There is general agreement that the Ivrea gabbro originated from mantle-derived melts, but the original chemical characteristics are obscured by large-scale contamination of the magma by crustal material (Voshage *et al.*, 1990; Mazzuchelli *et al.*, 1992*a*; Sinigoi *et al.*, 1994). The tholeiitic character of the Braccia and the Sondalo gabbros (Tribuzio *et al.*, 1999*a*) indicates upwelling and decompression melting of hot mantle rocks in Permian times. In fact, isotope studies in the Ligurian ophiolites by Rampone *et al.* (1998) revealed that Permian partial melting of asthenospheric mantle produced MORB-type tholeiitic melts similar to the parental Braccia gabbro melt. It is suggested that asthenosphere upwelling was associated with large-scale extension in the lithosphere (Fig. 9). On the basis of gabbro petrology (Rivalenti *et al.*, 1984) and syn-magmatic deformation (Quick *et al.*, 1992) it was suggested that mafic underplating in the Ivrea gabbros occurred in an extensional regime. Extension during and immediately after the intrusion is documented in subsolidus granulite facies flaser textures of the Braccia gabbro (Hermann & Müntener, 1996) and in a slight decompression of gabbro and country rocks during cooling (Müntener *et al.*, 2000). Permian extension at upper-crustal levels is documented in graben formation (Bertotti *et al.*, 1993).

The Braccia gabbro parental melt has a low LREE/HREE and $HREE_N$ of ~15–20 (Fig. 8) indicating that mantle partial melting originated within the spinel peridotite field. Consequently, the lithosphere must have been thinned in Permian times (Fig. 9). The mafic melts caused widespread partial melting of the lower crust and the granitic melts escaped to higher crustal levels (Voshage *et al.*, 1990; Sinigoi *et al.*, 1995; Hermann *et al.*, 1997). Thus, advective heat transfer by magmatism, rise of hot mantle rocks and the associated extension increased the geothermal gradient in Permian times.

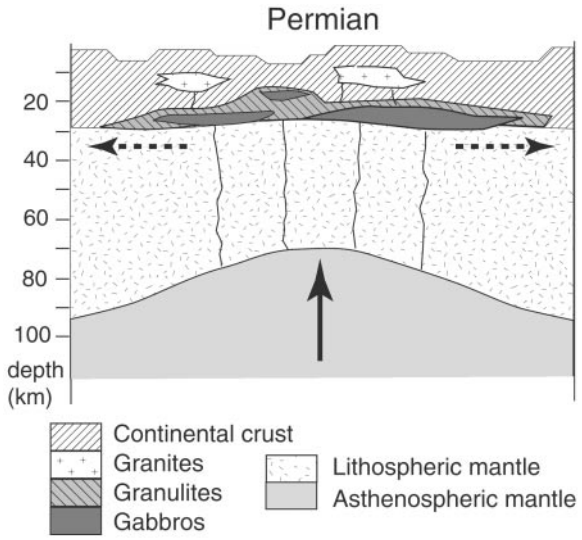

Fig. 9. Schematic illustration explaining mafic underplating and Permian extension with mantle upwelling. Gabbros were emplaced at the crust–mantle boundary (Malenco), in lower-crustal (Ivrea) and mid-crustal (Sondalo) levels. The mafic underplating led to partial melting of the lower crust and to the formation of granulites. The granitic partial melts form igneous bodies in mid- and upper-crustal levels.

CONCLUSIONS

The Braccia gabbro originated from an *in situ* type of crystallization (Langmuir, 1989) of tholeiitic magma at the base of the continental crust. Differentiation was driven mainly by the formation of gabbro–norite cumulates with various amount of trapped liquid. Trapped liquid equilibrated completely with cumulus minerals, thereby destroying compositional zoning of the minerals. Small amounts of trapped liquids can significantly affect mineral trace element composition. We have shown that the combination of mineral trace element modelling with the *mg*-number of pyroxenes allows us to estimate the amount of trapped liquid as well as the degree of differentiation. In the Braccia gabbro complex pure cumulates as well as frozen liquids exist. A particular feature is the absence of Cr-spinel–olivine ultramafic cumulates. This indicates that significant amounts of olivine fractionated before emplacement at the crust–mantle boundary.

The parental melt of the Braccia gabbro was recalculated from the most primitive pure cumulate found. The parental melt is very similar to T-MORB although the Braccia gabbro was emplaced at the base of the

continental crust and not in the oceanic crust. It most probably originated from decompression melting of upwelling spinel peridotites. This indicates that the lithosphere in the Permian time was thinned and that the geothermal gradient was high. Tholeiitic magmatism is one among several features providing evidence for extension on the northern edge of the African plate in Permian times.

ACKNOWLEDGEMENTS

This work was financially supported by the Swiss National Foundation grant 2000-037388·93/1. We thank P. Ulmer for fruitful discussion and careful corrections of an earlier version of this manuscript, and V. Trommsdorff and G. B. Piccardo for supervision during the Ph.D. work of J.H. and O.M. The paper benefited from suggestions by P. Kelemen, G. Yaxley, D. Rubatto and S. Eggins. We gratefully acknowledge the critical comments by A. Klügel and G. Rivalenti, which led to a significant improvement of the paper. We also thank E. Rampone and an anonymous reviewer for their careful reviews. H. Cousin provided some of the LAM-ICP-MS analyses. Special thanks go to Ch. Moor (EMPA Dübendorf) for his help with bulk-rock ICP-MS analysis.

REFERENCES

Barnes, S. J. (1986). The effect of trapped liquid crystallization on cumulus mineral compositions in layered intrusions. *Contributions to Mineralogy and Petrology* **93**, 524–531.

Bertotti, G., Picotti, V., Bernoulli, D. & Castellarin, A. (1993). From rifting to drifting: tectonic evolution of the South-Alpine upper crust from the Triassic to the early Cretaceous. *Sedimentary Geology* **86**, 53–76.

Bindeman, I. L., Davis, A. M. & Drake, M. J. (1998). Ion microprobe study of plagioclase–basalt partition experiments at natural concentration levels of trace elements. *Geochimica et Cosmochimica Acta* **62**, 1175–1193.

Cawthorn, R. G. (1996). Models for incompatible trace-element abundances in cumulus minerals and their application to plagioclase and pyroxenes in the Bushveld Complex. *Contributions to Mineralogy and Petrology* **123**, 109–115.

Elthon, D. & Scarfe, C. M. (1984). High-pressure phase equilibria of a high-magnesia basalt and the genesis of primary oceanic basalts. *American Mineralogist* **69**, 1–15.

Green, D. H. & Ringwood, A. E. (1967). The genesis of basaltic magmas. *Contributions to Mineralogy and Petrology* **15**, 103–190.

Günther, D., Frischknecht, R., Heinrich, C. A. & Kahlert, H. J. (1997). Capabilities of an argon fluorite 193 nm excimer laser for laser ablation inductively coupled plasma mass spectrometry microanalysis of geological materials. *Journal of Analytical Atomic Spectrometry* **12**, 939–944.

Hansmann, W., Hermann, J. & Müntener, O. (1996). U–Pb Datierung des Fedozer Gabbros, einer Intrusion an der Krusten Mantel Grenze. *Schweizerische Mineralogische und Petrographische Mitteilungen* **76**, 116–117.

Hauri, E. H., Wagner, T. P. & Grove, T. L. (1994). Experimental and natural partitioning of Th, U, Pb and other trace elements between garnet, clinopyroxene and basaltic melts. *Chemical Geology* **117**, 149–166.

Hermann, J. (1997). The Braccia gabbro (Malenco, Alps): Permian intrusion at the crust to mantle interface and Jurassic exhumation during rifting. Ph.D. thesis, ETH-Zürich.

Hermann, J. & Müntener, O. (1996). Exhumation-related structures in the Malenco–Margna system: implications for paleogeography and its consequences for rifting and Alpine tectonics. *Schweizerische Mineralogische und Petrographische Mitteilungen* **76**, 501–520.

Hermann, J., Müntener, O., Trommsdorff, V., Hansmann, W. & Piccardo, G. B. (1997). Fossil crust to mantle transition, Val Malenco (Italian Alps). *Journal of Geophysical Research* **102**, 20123–20132.

Kelemen, P. B., Koga, K. & Shimizu, N. (1997). Geochemistry of gabbro sills in the crust–mantle transition zone of the Oman ophiolite: implications for the origin of the oceanic lower crust. *Earth and Planetary Science Letters* **146**, 475–488.

Langmuir, C. H. (1989). Geochemical consequences of *in situ* crystallization. *Nature* **340**, 199.

Langmuir, C. H., Klein, E. M. & Plank, T. (1992). Petrological systematics of mid-ocean ridge basalts: constraints on melt generation beneath ocean ridges. In: Morgan, J. P., Blackman, D. K. & Sinton, M. J. (eds) *Mantle Flow and Melt Generation at Mid-Ocean Ridges. Geophysical Monograph, American Geophysical Union* **71**, 183–280.

Longerich, H. P., Jackson, S. E. & Günther, D. (1996). Laser ablation inductively coupled plasma mass spectrometric transient signal data acquisition and analyte concentration calculation. *Journal of Analytical Atomic Spectrometry* **11**, 899–904.

MacBirney, A. R. (1975). Differentiation of the Skaergaard intrusion. *Nature* **253**, 691–694.

Mazzucchelli, M., Rivalenti, G., Vannucci, R., Bottazzi, P., Ottolini, L., Hofmann, A. W. & Parenti, M. (1992a). Primary positive Eu anomaly in clinopyroxenes of low-crust gabbroic rocks. *Geochimica et Cosmochimica Acta* **56**, 2363–2370.

Mazzucchelli, M., Rivalenti, G., Vannucci, R., Bottazzi, P., Ottolini, L., Hofmann, A. W., Sinigoi, S. & Demarchi, G. (1992b). Trace element distribution between clinopyroxene and garnet in gabbroic rocks of the deep crust: an ion microprobe study. *Geochimica et Cosmochimica Acta* **56**, 2371–2385.

Müntener, O. & Hermann, J. (1996). The Val Malenco lower crust–upper mantle complex and its field relations (Italian Alps). *Schweizerische Mineralogische und Petrographische Mitteilungen* **76**, 475–500.

Müntener, O., Hermann, J. & Trommsdorff, V. (2000). Cooling history and exhumation of lower crustal granulites and upper mantle (Malenco, Eastern Central Alps). *Journal of Petrology* **41**, 175–200.

Piccardo, G. B. (1995). Ophiolites. In: Ranalli, G. (ed.) *Plate Tectonics: The First Twenty-Five Years. Proceedings VIII Summer School Earth and Planetary Sciences, Siena*, pp 267–296.

Puschnig, A. R. (1998). The Forno unit (Rhetic Alps): evolution of an ocean floor sequence from rifting to Alpine orogeny. Ph.D. thesis, ETH-Zürich.

Quick, J. E., Sinigoi, S. Negrini, L., Demarchi, G. & Mayer, A. (1992). Synmagmatic deformation in the underplated igneous complex of the Ivrea–Verbano zone. *Geology* **20**, 613–616.

Rampone, E., Hofmann, A. W. & Raczek, I. (1998). Isotopic contrasts within the Internal Liguride ophiolite (N. Italy): the lack of a genetic mantle–crust link. *Earth and Planetary Science Letters* **163**, 175–189.

Rivalenti, G., Garuti, G., Rossi, A., Siena, F. & Sinigoi, S. (1981). Existence of different periodite types and of a layered igneous complex of the Ivrea Verbano zone of the Western Alps. *Journal of Petrology* **22**, 127–153.

Rivalenti, G., Rossi, A., Siena, F. & Sinigoi, S. (1984). The layered series of the Ivrea–Verbano igneous complex, western Alps, Italy. *Tschermarks Mineralogische und Petrographische Mitteilungen* **33**, 77–99.

Schosnig, M. & Hoffer, E. (1998). Compositional dependence of REE partitioning between diopside and melt at 1 atmosphere. *Contributions to Mineralogy and Petrology* **133**, 205–216.

Sinigoi, S., Quick, J. E., Clemens-Knott, D., Mayer, A., Demarchi, G., Mazzuchelli, M., Negrini, L. & Rivalenti, G. (1994). Chemical evolution of a large mafic intrusion in the lower crust, Ivrea–Verbano Zone, Northern Italy. *Journal of Geophysical Research* **99**, 21575–21590.

Sinigoi, S., Quick, J. E., Mayer, A. & Demarchi, G. (1995). Density-controlled assimilation of underplated crust, Ivrea–Verbano zone, Italy. *Earth and Planetary Science Letters* **129**, 183–191.

Sun, S. S. & McDonough, W. F. (1989). Chemical and isotope systematics of oceanic basalts: implications for mantle composition and processes. In: Saunders, A. D. & Norry, M. J. (eds) *Magmatism in the Ocean Basins. Geological Society, London, Special Publications*, **42**, 313–345.

Sun, S. S., Nesbitt, R. W. & Sharaskin, A. Y. (1979). Geochemical characteristics of mid-ocean ridge basalts. *Earth and Planetary Science Letters* **44**, 119–138.

Thompson, R. N., Morrison, M. A., Hendry, G. L. & Parry, S. J. (1984). An assessment of the relative roles of crust and mantle in magma genesis. *Philosophical Transactions of the Royal Society of London, Series A* **310**, 549–590.

Tribuzio, R., Thirlwall, M. F. & Messiga, B. (1999a). Petrology, mineral and isotope geochemistry of the Sondalo gabbroic complex (Central Alps, Northern Italy): implications for the origin of post-Variscan magmatism. *Contributions to Mineralogy and Petrology* **136**, 48–62.

Tribuzio, R., Tiepolo, M., Vannucci, R. & Bottazzi, P. (1999b). Trace element distribution within olivine-bearing gabbros from the Northern Apennine ophiolites (Italy): evidence for post-cumulus crystallization in MOR-type gabbroic rocks. *Contributions to Mineralogy and Petrology* **134**, 123–133.

Trommsdorff, V., Piccardo, G. B. & Montrasio, A. (1993). From magmatism through metamorphism to sea floor emplacement of subcontinental Adria lithosphere during pre-Alpine rifting (Malenco, Italy). *Schweizerische Mineralogische und Petrographische Mitteilungen* **73**, 191–203.

Ulrich, T. (1995). Strukturelle und petrographische Untersuchungen im oberen Val Malenco. Teil 2. Diploma thesis, ETH-Zurich.

Ulrich, T. & Borsien, G. R. (1996). Chemische Untersuchungen am Fedozer Gabbro und ein Vergleich mit dem Forno Metabasalt (Val Malenco, Norditalien). *Schweizerische Mineralogische und Petrographische Mitteilungen* **76**, 521–535.

Venturelli, G., Thorpe, R. S. & Potts, P. J. (1981). Rare earth and trace element characteristics of ophiolitic metabasalts from the Alpine–Apennine belt. *Earth and Planetary Science Letters* **53**, 109–123.

Voshage, H., Hofmann, A. W., Mazzucchelli, M., Rivalenti, G., Sinigoi, S., Raczek, I. & Demarchi, G. (1990). Isotopic evidence from the Ivrea zone for a hybrid lower crust formed by magmatic underplating. *Nature* **347**, 731–736.

Wells, P. R. A. (1977). Pyroxene thermometry in simple and complex systems. *Contributions to Mineralogy and Petrology* **62**, 129–139.